Arch Appl Mech (2015) 85:339–345
DOI 10.1007/s00419-014-0957-4

SPECIAL

Fei Hui · Yuanyuan Shi · Yanfeng Ji · Mario Lanza · Huiling Duan

Mechanical properties of locally oxidized graphene electrodes

Received: 3 January 2014 / Accepted: 28 March 2014 / Published online: 21 November 2014

Abstract Graphene has many outstanding mechanical, electronic and optical properties, which makes it an ideal material for future transparent-flexible electronic devices. In such applications, graphene is exposed to atmospheric conditions and must withstand high mechanical stresses without forming cracks or discontinuities, so that the electrical current can flow along it. Although graphene is a very resistant material, local oxidation of graphene may alter its pristine structure, leading to a lower mechanical strength and high risk of fracture. Here, we analyze the mechanical properties of graphene in oxidative environments using a wide range of nanoscale tools and performing accelerated oxidation tests. Our experiments indicate that local oxidation of graphene sheets may alter its mechanical properties, leading to soft locations that easier to indent and increase the frictional coefficient of the sheets.

Keywords Graphene · Local oxidation · Mechanical properties · Hillock · Plateau

1 Introduction

Graphene is a novel material that consists of a two-dimensional sheet of carbon atoms arranged in a dense hexagonal lattice structure [1], and it has been found that it shows excellent mechanical, physical and electronic properties [2–5]. Although it has attracted the attention of many researchers and companies, graphene has still not been introduced in real industrial processes. The main reason is that the there is still no efficient method to produce graphene sheets with controllable thicknesses, sizes and defects on silicon. Moreover, the fabrication of graphene-based devices requires some photolithography steps [6,7], which may impoverish its performance due to contamination. On the other hand, graphene has been suggested as conductive, flexible and transparent electrode for future electronic applications like rollable nanogenerators [8] and species sensors [9], where the graphene sheet should withstand the external mechanical stresses induced by the device movement. In those cases, graphene films are normally grown by chemical vapor deposition (CVD) [10] on different metals and transferred on transparent polymers like poly-methyl methacrylate (PMMA) or polydimethylsiloxane (PDMS), forming a transparent stack that can drive electric current along its surface. Since in those applications, graphene sheets are exposed to oxidation in air atmosphere, and since the physical continuity of the graphene is essential for a good performance as electrode, the effect of oxidative environments on the properties of graphene should be further studied.

F. Hui · Y. Shi · Y. Ji · M. Lanza
Institute of Functional Nano and Soft Materials, Soochow University, 199 Ren-Ai Road, Suzhou, Industrial Park, Suzhou, 215123 Jiangsu, China
E-mail: mlanza@suda.edu.cn

H. Duan (✉)
State Key Laboratory for Turbulence and Complex System, CAPT, Department of Mechanics and Engineering Science, College of Engineering, Peking University, Beijing 100871, China
E-mail: hlduan@pku.edu.cn

Due to its dense structure, graphene has the property of impeding other particles to flow through it [7], which can be used to passivate the surface of other materials [11]. In particular, graphene has been shown to protect the surface of Cu and Ni [12] in air environment [13], in hydrogen peroxide [8] and even at high temperatures [14,15]. However, graphene structure is not perfect due to the often presence of defects, which may let oxygen atoms from the atmosphere locally oxidize the graphene sheet. In this work, we use the scanning electron microscope (SEM), Auger electron spectroscopy (AES) and conductive atomic force microscope (CAFM) to examine the performance of graphene single layer (GSL) exposed to accelerated oxidation tests in hydrogen peroxide (H_2O_2), focusing on the mechanical properties of fresh and oxidized locations.

2 Experimental

We use as-grown graphene single layer (GSL) on copper from ACS Materials Llc. The sample was immersed in Hydrogen Peroxide (H2O2) from Sinopharm Chemical Reagent Co., Ltd for 1 h. After that, the Quanta 200FEG Scanning Electron Microscope was used to characterize the surface of as-grown and treated GSL/Cu samples, using an intensity signal of 15KV. The chemical composition of the different locations at the sample surface is analyzed using the PHI 700 AES. Topographic and mechanical nanoscale characterization was made with a Veeco Multimode V CAFM working in air atmosphere. The surface of the sample was scanned in contact mode using Pt–Ir-coated silicon tips from Bruker (model SCM-PIC). The force–distance (F-D) curves were locally performed at the samples to analyze their adhesion force. In addition, we use nano-indentation analysis using a TriboIndenter with a standard 50-nm Berkovich diamond tip combined with AFM maps. The AFM images were processed with the WSxM software (version 5.0 develop 6.5) from Nanotec.

3 Results and discussion

Monolayer sheets of graphene were grown on 25-μm-thick copper foils (purchased from Alfa Aesar, item No. 13382) by a low-pressure chemical vapor deposition (LPCVD) method [16]. We introduced the copper foil in a tube furnace and a 1 in. diameter quartz tube, and we annealed it at 1,030 °C during 1 h under a 20 standard cubic centimeters per minute (sccm) H_2 flow with the aim of removing surface oxides. After this, methane (10 sccm) was introduced into the system to grow graphene for 20–30 min. Using this methodology, other authors produced GSL layer sheets with graphene domains with diameters of 1–3 μm [17–21]. We corroborate the monolayer nature of our graphene sheets with Raman Spectroscopy [22,23].

Polycrystalline GSL grown by CVD on 25-μm-thick copper foils was first characterized using SEM and topographic AFM in contact mode. Figure 1 shows the typical SEM (a) and three-dimensional AFM (b) images of as-grown GSL/Cu sample. As it can be observed, the typical copper steps and copper grain boundaries can be identified from both images. These features are characteristic of GSL-on-Copper, and they are generated by the high temperature used during the CVD growth of graphene [24]. The graphene domains cover large areas with diameters always above 50 μm, and the average copper steps are ∼20 nm tall and ∼400 nm width. On the other hand, when a GSL/Cu stack is exposed to an oxidative environment (H_2O_2), its morphology remarkably changes. As an example, Fig. 1 SEM image (c) and three-dimensional AFM images (d) of treated GSL/Cu sample soaked in H_2O_2 for 1 h. It is not difficult to observe that the topography of the treated samples has been changed: A large amount of hillocks appeared on the surface of the sample. It is interesting to highlight that these features seem to be following circular paths with diameters around 1-3 μm, similar to the graphene domains, indicating that the hillocks may only form at the graphene domain boundaries. We also characterized the height, width and density of these hillocks by doing statistical analysis of the AFM topographic images, using the AFM software. Figure 2 shows the histogram of the (a) area (b) width and (c) height of the hillocks that appeared in the GSL/Cu sample that was immersed in H_2O_2 for 1 h. Images 2(b) and 2(c) show us that the mean width of these hillocks is 215 nm and the mean height is 10 nm. Figure 2a is a 8.4 μm × 14.4 μm, and the value of the area covered by the oxidation paths is 23.61 %. This calculation has been made using a threshold slightly above the mean topographic value of the plateaus.

To be completely sure that these features are related to the H_2O_2 treatment, we partially immersed a fresh GSL/Cu sample in the H_2O_2 for 1 h and we measured topographic AFM scans at the border. Figure 3a shows the corresponding topographic AFM map at the immersion border. It is worth noting that the corrugations only formed at the immersed area, where the surface roughness increased dramatically, while the part of the sample not soaked in H_2O_2 still kept its original flat morphology.

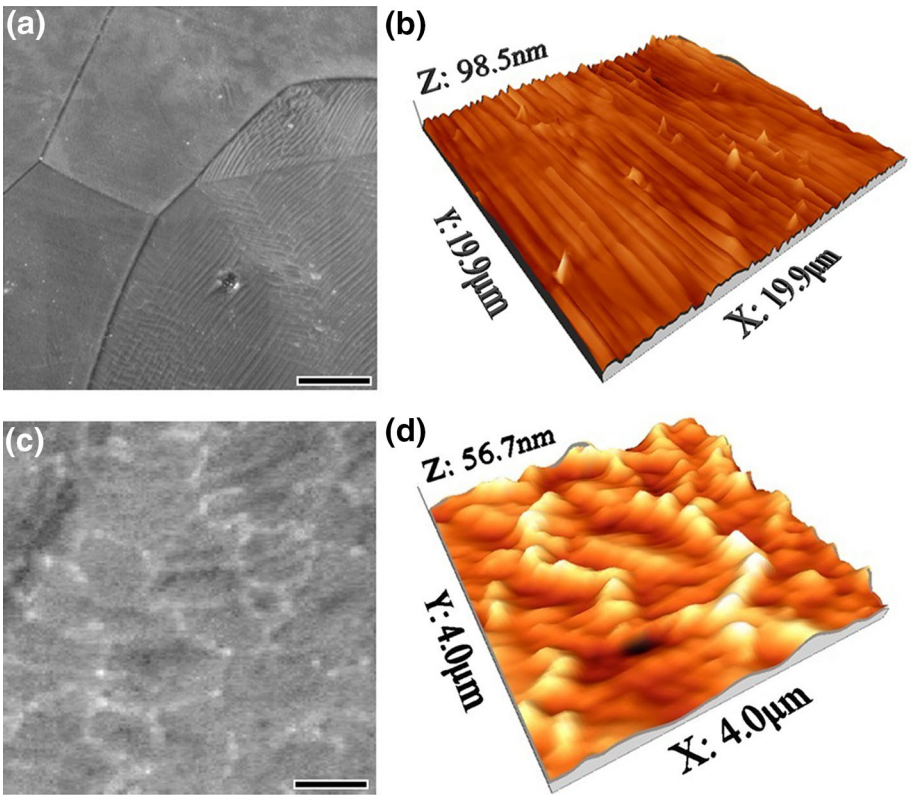

Fig. 1 SEM image (**a**) and AFM image (**b**) of as-grown (not treated) GSL/Cu sample. The copper steps and copper grain boundaries can be distinguished clearly. SEM image (**c**) and AFM image (**d**) of treated GSL/Cu sample soaked in H_2O_2 for 1 h. Many bright spots formed, and AFM image corroborates that they are hillocks. Hillock formation seems to follow the typical path of the graphene domains. The *scale bar* in (**a**) and (**c**) are 10 and 2 μm, respectively

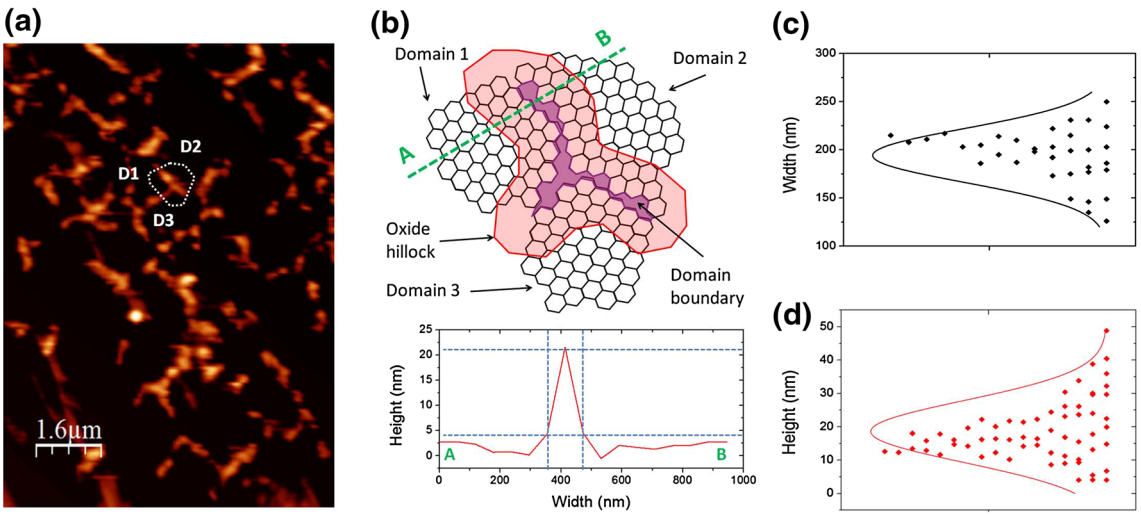

Fig. 2 Example of a statistical analysis of the (**a**) area covered by the oxide hillocks that appeared in the GSL/Cu sample that was immersed in H_2O_2 for 1 h. The amount of the area covered by the oxidation paths in (**a**) is 23.61 %. (**b**) shows a schematic of the *dashed area* in (**a**), and it represents the formation and propagation of the oxide hillock around the domain boundary. The graph in (**b**) shows one example of a real cross section in a region similar to the A-B line in the schematic. **c** and **d** Show the statistical analyses of the width (**c**) and height (**d**) of the hillocks. These parameters are highlighted in (**b**) with *blue-dashed lines*. (Color figure online)

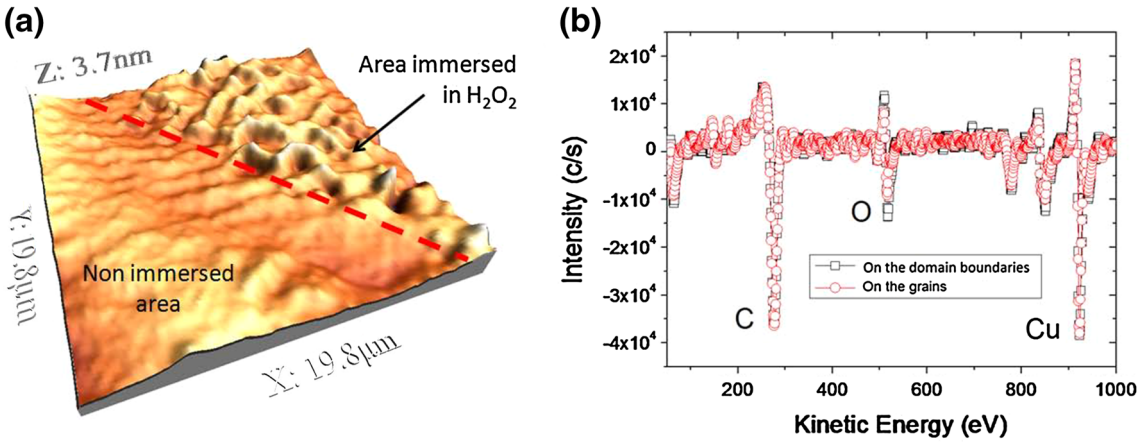

Fig. 3 The AFM image (**a**) of the GSL/Cu sample is partially immersed in H_2O_2 (during 1 h). It shows that the hillocks only formed in the immersed area. **b** The typical AES survey displaying the chemical composition on the domain boundaries and on the plateaus of the GSL/Cu stack that was soaked in H_2O_2 for 1 h

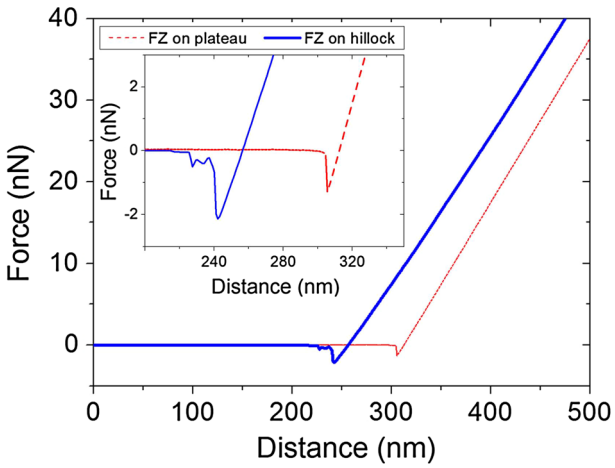

Fig. 4 Typical backward force–distance curve performed with the tip of the CAFM on a hillock (oxidized area, *thick-blue continuous line*) and on a plateau (non-oxidized area, *red-thin dashed line*). The *inset* shows the more zoom of the negative peaks. The instabilities and more negative peak on the hillock reveal that it is more sticky than the plateau. (Color figure online)

In the next step, we analyze the chemical composition on the hillocks and plateaus of the GSL/Cu sample soaked in H_2O_2 for 1 h using AES. The typical surveys showing the main chemical signals measured on the hillocks and on the plateaus of the treated sample are shown in Fig. 3b. The AES intensity versus kinetic energy plot clearly shows an increase in the oxygen peak when measuring on the hillocks, while the carbon and copper peaks show no significant differences on both locations. Therefore, the immersion of the GSL/Cu sample in H_2O_2 produces high concentration of oxygen at the surface of the sample. As shown in Fig. 1c, these oxygen hillocks seem to appear only at the GSL domain boundaries; the missing bonds related to the pentagonal and heptagonal defects at the GSL domain boundaries may let oxygen atoms effectively bond with the carbon/copper atoms [25,26], which represents the onset of the oxygen accumulation at those locations.

Finally, we analyze the mechanical performance of the graphene sheets after the treatment. Figure 4 shows the typical result obtained when applying backward F–D curves with the tip of the AFM on a plateau (non-oxidized) and on a hillock (oxidized area), respectively. As it can be observed, the magnitude of the backward peak on the hillock (−2.2 nN) is higher than the one on the plateau (−1.2 nN). It has been reported that the negative peak at the AFM backward (retract) force–distance curve corresponds to the adhesion force between the tip and the sample [27–29]. Therefore, the adhesion force between tip and the sample is larger at the hillock. Such increase in the adhesion force may be related to two different phenomena. The first is that the oxide hillocks are more sticky than the flat graphene. Although it has been recently demonstrated that graphene adhesion to a silicon substrate is much larger than that of typical micromechanical structures [30], this has

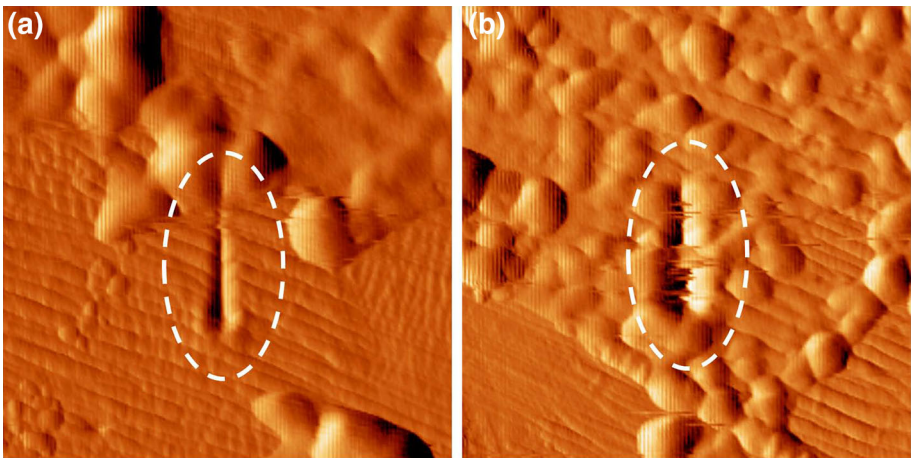

Fig. 5 AFM-like images measured with the tip of the nano-indentation tool after a vertical stress of 500 nN on the plateau (**a**) and on the hillock (**b**). The *white circles* indicate the indentation locations

been attributed to an high degree of adhesion between both layers because graphene high flexibility lets it adapt better to the silicon substrate, increasing the contact area and the adhesion by Wan der Waals forces. This result does not apply to our experiment, since graphene is already on a substrate and it cannot adapt to the morphology of our tip. On the other hand, sticky materials are known to have weaker bonds, and since graphene has been shown to be a very stable material [31], it is reasonable to think that the oxide hillocks are more sticky (in contact with the AFM tip) than pristine graphene. The second is that the contact areas between the tip and the sample at both locations would be different. Different contact models, such as Hetzt and Sheddon, Derjaguin–Miller–Toporov, Bradley, Maugis, and Johnson–Kendall–Roberts (summarized in references [29,32–34]), have been used to describe the interaction between the CAFM tip and solid rigid samples, and the most commonly used in AFM studies similar to the one presented here is Hetzt and Sheddon [29,35,36]. In this model, the contact force between the tip and the sample increases with the tip radius. On the other hand, it has been demonstrated that larger contact areas in AFM experiments lead to larger adhesion forces. Frammelsberber et al. [36] demonstrated (from force–distance curves) that the adhesion force between diamond-doped AFM tips (with typical radius of 200 nm) and a bare piece of SiO_2/Si is larger than when using platinum–iridium AFM tips (with typical radius of 20 nm). Therefore, the increase in area (probably generated by tip penetration in the hillock) may be the reason for the increase in the adhesion force observed in Fig. 4. Interestingly, there is a fluctuate part on the hillock curve while no one on the plateau curve, which indicates that the adhesion force between the tip and the oxide produces some partial bond ruptures [27]. Moreover, the slope of the curve at the linear part on the hillock is slightly lower than on the plateau. Since that part of the curve corresponds to the time in which the tip is in contact to the sample, this result is indicating that the surface of the hillock can be slightly deformed (perforated) during the FZ curve, pointing out its mechanical weakness. This observation is further supporting the theory that the increase in the adhesion force of the sample is related to a larger tip/sample contact area (perforating the hillock may lead to a larger tip/sample contact area).

Nano-indentation tests further supported this hypothesis and also revealed additional information. Vertical tests were performed with the tip of the nano-indentation by applying the same contact force at both hillocks and plateaus, and the deformation (hole) produced by the stiff tip is analyzed. Figure 5a, b show the AFM-like images recorded with the nano-indentation tool after the vertical stress applied on the plateau and on the hillocks, respectively. The results indicate that, while original graphene can withstand the mechanical stress induced by the tip, oxidized areas are weaker and the tip can easily penetrate on the hillock, leading to an indent on the top.

4 Conclusions

GSL/Cu stacks can be locally oxidized when exposed to oxidative environments. By means of SEM, AFM and AES, it has been observed that tall and wide hillocks made of oxygen can grow along the graphene domain boundaries. On the other hand, the genuine hexagonal lattice of graphene in the domains effectively

remains unaltered by the oxygen. Our experiments also verified that the local oxidation dramatically affects the mechanical performance of the graphene layer.

Acknowledgments The following agencies and programs are acknowledged: Major State Basic Research Development Program of China (Grant no. 2011CB013101), National Natural Science Foundation of China (NSFC) under Grants 11225208, 11172001, 10872003, and 11072230. Huiling Duan would like to acknowledge the Alexander von Humboldt (AvH) foundation in Germany to support this work through project "Mechanics theory of materials with complex surfaces and its applications" in the frame of the AvH program for funding a research group linkage.

References

1. Castro Neto, A.H., Guinea, F., Peres, N.M.R., Novoselov, K.S., Geim, A.K.: The electronic properties of Graphene. Rev. Mod. Phys. **81**, 109–162 (2009)
2. Li, X.L., Zhang, G.Y., Bai, X.D., Sun, X.M., Wang, X.R., Wang, E., Dai, H.J.: Highly conducting graphene sheets and Langmuir–Blodgett films. Nat. Nanotechnol. **3**, 538–542 (2008)
3. Novoselov, K.S., Geim, A.K., Morozov, S.V., Jiang, D., Zhang, Y., Dubonos, S.V., Grigorieva, I.V., Firsov, A.A.: Electric field effect in atomically thin carbon films. Science **306**, 666–669 (2004)
4. Lanza, M., Wang, Y., Bayerl, A., Gao, T., Porti, M., Nafria, M., Liang, H., Jing, G., Zhang, Y., Tong, H., Duan, H.: Tuning graphene morphology by substrate towards wrinkle-free devices: experiment and simulation. J. Appl. Phys. **113**, 104301 (2013)
5. Peres, N.M.R.: Colloquium: the transport properties of graphene: an introduction. Rev. Mod. Phys. **82**, 2673–2700 (2010)
6. Lanza, M., Wang, Y., Bayerl, A., Gao, T., Porti, M., Nafria Zhou, Y., Jing, G., Liu, Z., Zhang, Y., Dapeng, Y., Duan, H.: Electrical and mechanical performance of graphene sheets exposed to oxidative environments. Nano Res. **6**(7), 485–495 (2013)
7. Novoselov, K.S., Fal'ko, V.I., Colombo, L., Gellert, P.R., Schwab, M.G., Kim, K.: Aroadmap for graphene. Nature **490**, 192–200 (2012)
8. Choi, D., Choi, M.Y., Choi, W.M., Shin, H.J., Park, H.K., Seo, J.S., Park, J., Yoon, S.M., Chae, S.J., Lee, Y.H., Kim, S.W., Choi, J.Y., Lee, S.Y., Kim, J.M.: Fully rollable transparent nanogenerators based on graphene electrodes. Adv. Mater. **22**, 2187–2192 (2010)
9. Basu, P.K., Indukuri, D., Keshavan, S., Navratna, V., Vanjari, S.R.K., Raghavan, S., Bhat, N.: Graphene based *E.coli* sensor on flexible acetate sheet. Sens. Actuators B Chem. **190**, 342–347 (2014)
10. Li, X.S., Carl, W., Magnuson Venugopal, A., Tromp, R.M., Hannon, J.B., Vogel, E.M.L. Colombo, Ruoff, R.S.: Large-area graphene single crystals grown by low-pressure chemical vapor deposition of methane on copper. J. Am. Chem. Soc. **133**, 816–2819 (2011)
11. Chen, S., Brown, L., Levendorf, M., Cai, S., Ju, S.Y., Edgeworth, J., Li, X., Magnuson, C.W., Velamakanni, A., Piner, R.D., Kang, J., Park, J., Ruoff, R.S.: Oxidation resistance of graphene-coated Cu and Cu/Ni alloy. ACS Nano. **5**(2), 1321–1327 (2011)
12. Li, X.S., Cai, W.W., An, J.H., Kim, S., Nah, J., Yang, D.X., Piner, R.D., Velamakanni, A., Jung, I., Tutuc, E., Banerjee, S.K., Colombo, L., Ruoff, R.S.: Large-area synthesis of high-quality and uniform graphene films on copper foils. Science **324**, 1312–1314 (2009)
13. Duong, D.L., Han, G.H., Lee, S.M., Gunes, F., Kim, E.S., Kim, S.T., Kim, H., Ta, Q.H., So, K.P., Yoon, S.J., Chae, S.J., Jo, J.W., Park, M.H., Chae, S.H., Lim, S.C., Choi, J.Y., Lee, Y.H.: Probing graphene grain boundaries with optical microscopy. Nature **490**, 235–239 (2012)
14. Kang, D., Kwon, J.Y., Cho, H., Sim, J.H., Hwang, H.S., Kim, C.S.: Oxidation resistance of Iron and copper foils coated with reduced graphene oxide multilayers. ACS Nano. **6**(9), 7763–7769 (2012)
15. Nilsson, L., Andersen, M., Balog, R., Laegsgaard, E., Hofmann, P., Besenbacher, F., Hammer, B., Stensgaard, I., hornekaer, L.: Graphene coatings: probing the limits of the one atom thick protection layer. ACS Nano. **6**(11), 10258–10266 (2012)
16. Ahmad, M., Han, S.A., Tien, D.H., Jung, J., Seo, Y.: Local conductance measurement of graphene layer using conductive atomic force microscopy. J. Appl. Phys. **110**, 054307 (2011)
17. Kwon, S., Chung H., J., Seo, S., Park, J.Y.: Domain structures of single layer graphene imaged with conductive probe atomic force microscopy. Surf. Interface Anal. **44**, 768–771 (2012)
18. Orofeo, C.M., Hibino, H., Kawahara, K., Ogawa, Y., Tsuji, M., Ikeda, K.I., Mizuno, S., Ago, H.: Influence of Cu metal on the domain structure and carrier mobility in single-layer graphene. Carbon **50**, 2189–2196 (2012)
19. Ismach, A., Druzgalski, C., Penwell, S., Schwartzberg, A., Zheng, M., Javey, A., Bokor, J., Zhang, Y.G.: Direct chemical vapor deposition of graphene on dielectric surfaces. Nano Lett. **10**, 1542–1548 (2010)
20. Han, G.H., Günes, F., Bae, J.J., Kim, E.S., Chae, S.J., Shin, H.J., Choi, J.Y., Pribat, D., Lee, Y.H.: Influence of copper morphology in forming nucleation seeds for graphene growth. Nano Lett. **11**, 4144–4148 (2011)
21. Robertson, A.W., Warner, J.H.: Hexagonal single crystal domains of few-layer graphene on copper foils. Nano Lett. **11**, 1182–1189 (2011)
22. Lanza, M., Gao, T., Yin, Z.X., Zhang, Y.F., Liu, Z.F., Tong, Y.Z., Shen, Z.Y., Duan, H.L.: Nanogap based graphene coated AFM tips with high spatial resolution conductivity and durability. Nanoscale **5**, 10816–10823 (2013)
23. Lanza, M., Bayerl, A., Gao, T., Porti, M., Nafria, M., Jing, G., Zhang, Y., Liu, Z., Duan, H.: Graphene-coated Atomic Force Microscope tips for reliable nanoscale electrical characterization. Adv. Mater. **25**, 1440–1444 (2013)
24. Zhang Y., F., Gao, T., Gao, Y.B., Xie, S.B., Ji, Q.Q., Yan, K., Peng, H.: Defect-like structures of graphene on copper foils for strain relief investigated by high-resolution scanning tunneling microscopy. ACS Nano. **5**(5), 4014–4022 (2011)

25. Regan, W., Alem, N., Aleman, B., Geng, B., Girit, Caglar., Maserati, L., Wang, F., Crommie, M., Zettl, A.: A direct transfer of layer-area Graphene. Appl. Phys. Lett. **96**, 113102 (2010)
26. Mattevi, C., Kim, H., Chhowalla, M.: A review of chemical vapour deposition of graphene oncopper. J. Mater. Chem. **21**, 3324–3334 (2011)
27. Zivkovic, J.: AFM force spectroscopy of viral systems. PhD disertation Ipskamp Drukkers. 978-90-9027386-0 (2013)
28. Bhushan, B.: Springer Handbook of Nanotechnology. Springer, New York (2004)
29. Cappella, B., Dietler, G.: Force-distance curves by atomic force microscopy. Surf. Sci. Rep. **34**, 1–3 (1999)
30. Steven, P., Koenig Narasimha, G., Boddeti Martin, L., DunnScott, B.J.: Ultrastrong adhesion of graphene membranes. Nat. Nanotechnol. **6**, 543–546 (2011)
31. Shin, Y.J., Stromberg, R., Nay, R., Huang, H., Wee, A.T.S., Yang, H., Bhatia, C.S.: Frictional characteristics of exfoliated and epitaxial graphene. Carbon **49**, 4070–4073 (2011)
32. Kremmer, S., Peissl, S., Teichert, C., Kuchar, F.: Proceedings of the 28th International Symposium of Testing and Failure Analysis. EDFAS 473–482 (2002)
33. Kremmer, S., Peissl, S., Teichert, C., Kuchar, F., Hofer, H.: Modification and characterization of thin silicon gate oxides using conductive atomic force microscopy. Mater. Sci. Eng. **102**, 88–93 (2003)
34. Shi, X.H., Zhao, Y.P.: Comparison of various adhesion contact theories and the influence of dimensionless load parameter. J. Adhes. Sci. Technol. **18**, 55–68 (2004)
35. Olbrich A.: Characterisation of thin dielectrics by means of modified atomic force microscopy. PhD thesis University of Regensburg Regensburg Germany. (1999)
36. Frammelsberger, W., Benstetter, G., Kiely, J., Stamp, R.: C-AFM-based thickness determination of thin and ultra-thin SiO2 films by use of different conductive-coated probe tips. App. Surf. Sci. **253**, 3615–3626 (2007)